

Quantifying nonclassicality of mixed Fock states

Spencer Rogers,^{1,*} Tommy Muth,¹ and Wenchao Ge¹

¹*Department of Physics, University of Rhode Island, Kingston, RI 02881, USA*

(Dated: June 5, 2024)

Nonclassical states of bosonic modes are important resources for quantum-enhanced technologies. Yet, quantifying nonclassicality of these states, in particular mixed states, can be a challenge. Here we present results of quantifying the nonclassicality of a bosonic mode in a mixed Fock state via the operational resource theory (ORT) measure [W. Ge, K. Jacobs, S. Asiri, M. Foss-Feig, and M. S. Zubairy, *Phys. Rev. Res.* 2, 023400 (2020)], which relates nonclassicality to metrological advantage. Generally speaking, evaluating the ORT measure for mixed states is challenging, since it involves finding a convex roof. However, we show that our problem can be reduced to a linear programming problem. By analyzing the results of numerical optimization, we are able to extract exact, analytical results for the case where three or four neighboring Fock states have nonzero population. Interestingly, we find that such a mode can be in distinct phases, depending on the populations. Lastly, we demonstrate how our method is generalizable to density matrices of higher ranks. Our findings suggests a viable method for evaluating nonclassicality of arbitrary mixed bosonic states and potentially for solving other convex roof optimization problems.

I. INTRODUCTION

For bosonic modes in quantum optics and other analogous fields, the coherent states, defined as eigenstates of the annihilation operator, are regarded as the most classical [1]. Not only do they have minimal uncertainty and maintain their shape under the harmonic oscillator Hamiltonian, but also they remain separable from each other when subject to linear interactions (as occur in beam-splitters). By contrast, superpositions of coherent states (e.g., cat and squeezed states) may have highly nonclassical features, and with these the potential to revolutionize such technologies as communication [2], computation [3, 4], and metrology [5]. Indeed, on the metrological side, squeezed states have already become an important tool in advanced gravitational wave interferometry [6, 7].

Given the applications of nonclassicality, quantifying it, i.e., ranking the nonclassicality of different bosonic states, is an important problem. Various measures of nonclassicality have been proposed, including the nonclassicality depth [8], nonclassical distance [9, 10], quantifications in terms of the Schmidt rank [11, 12], and resource-theoretic measures [13–15]. These measures satisfy the basic criteria that they are non-negative, and zero only for classical states (i.e., coherent states or, if mixed, classical mixtures of coherent states). They also characterize meaningful aspects of nonclassicality, such as the minimum number of coherent superpositions in a quantum state (in the case of the Schmidt rank) [11].

Here, we focus on the operational resource theory (ORT) measure of nonclassicality [16, 17], which has two defining features. First, it is *operational*, since it is related to the usefulness of a state for certain tasks. For pure states, the ORT measure directly quantifies the

metrological power of a state in terms of the quantum Fisher information of quadrature sensing [18], while for mixed states, the ORT measure is a tight upper bound on this power; this is the closest possible relationship because some nonclassical mixed states have zero metrological advantage over coherent states. This feature endows the ORT measure an operational meaning to evaluate different nonclassical states on the same footing. Second, the ORT measure is *resource-theoretic*. A quantum resource theory [19] defines free states and resource states via the operations, called *free operations*, under which it is impossible to increase that resource. In the ORT measure of nonclassicality, coherent states, and classical mixtures of them, are considered the free states, while nonclassical states are considered resource states. The free operations are classical operations (meaning operations that cannot create superpositions of coherent states from mixtures of coherent states) — Ref. [16] rigorously showed that the ORT measure does not increase under such operations.

Previous works computed the ORT measure, from here on also referred to as the *nonclassicality* \mathcal{N} , for various pure bosonic states of interest [16, 17, 20]. It has been shown, for example, that squeezed vacuum has the highest nonclassicality per unit average energy (which speaks to the metrological usefulness of squeezed vacuum) [16]. Cat states whose nonclassicality per unit energy approach that of squeezed vacuum in the asymptotic limit of large energy have also been discovered [17], thus extending our knowledge of optimal sensing with Mach-Zehnder interferometry [16, 21].

While pure states are ideal for applications, *mixed* states are inevitable in practice, due to coupling to the environment. For example, mixtures of Fock states can be generated under a dephasing channel in various bosonic systems [22–24]. Computing the ORT measure for a mixed state $\hat{\rho}$, however, poses a significant challenge. This is because the ORT measure for mixed states is a convex roof construction, similar to entanglement mea-

* spencer.rogers@uri.edu

tures for mixed states [25, 26] — computing it involves extremizing a function over all the decompositions of $\hat{\rho}$. Previous calculations only address very simple classes of states [17]. For more general states, only a lower bound has been given: $\mathcal{N}(\hat{\rho}) \geq \mathcal{W}(\hat{\rho})$, where $\mathcal{W}(\hat{\rho})$ is the metrological power (to be defined later) [17]. In this work, we present a numerical method of linear programming for calculating the ORT measure for mixed Fock states. Based on the numerical results, we extract analytical ansatz of the ORT measure for rank-3 and rank-4 mixed states and identify distinct phases depending on the populations. Our method provides a viable way to evaluate arbitrary mixed states of bosonic systems.

Our paper is structured as follows: in section II, we review the ORT measure of nonclassicality for pure and mixed states. In section III, we explain our method, based on linear programming, for calculating the ORT measure for mixed states. We focus on one class of mixed states in particular: those that are diagonal in the Fock basis. In section IV, we apply our method to rank-3 and rank-4 states, and show that such states can be in various phases, depending on their populations. The results here are largely analytical, as we were able to infer exact values from the numerical results. For higher-rank states, numerical results are possible, as we demonstrate on truncated thermal states. Section V contains our concluding remarks.

II. THE ORT MEASURE

A. Pure states

A pure bosonic state $|\psi\rangle$ is defined as *nonclassical* if and only if it is not a coherent state, i.e., $\hat{a}|\psi\rangle \neq \alpha|\psi\rangle$ for all complex numbers α [1]. The ORT measure \mathcal{N} assigns a nonclassicality value to each pure state as [16, 17]:

$$\begin{aligned} \mathcal{N}(|\psi\rangle) &= \max_{\mu} \langle \psi | (\Delta \hat{X}_{\mu})^2 | \psi \rangle - \frac{1}{2} \\ &= \langle \hat{a}^{\dagger} \hat{a} \rangle - |\langle \hat{a} \rangle|^2 + |\langle \hat{a}^2 \rangle - \langle \hat{a} \rangle^2|. \end{aligned} \quad (1)$$

Here, $(\Delta \hat{X}_{\mu})^2$ is the variance of a quadrature $\hat{X}_{\mu} = i(e^{-i\mu}\hat{a}^{\dagger} - e^{i\mu}\hat{a})/\sqrt{2}$, \hat{a} is the annihilation operator for the mode and $\mu \in [0, 2\pi]$.

Whereas the second line in Eq. (1) is generally more convenient for calculations, the first line makes the connection to metrological power more apparent. In quantum metrology with unitary encoding, one measures a classical parameter θ by applying a transformation $\hat{U}(\theta) = e^{-i\theta\hat{G}}$ to a quantum sensor, where the generator \hat{G} is some Hermitian observable of the quantum sensor. $\hat{U}(\theta)$ may represent the effect of coupling the quantum sensor to a classical system, and may or may not describe some interaction picture. Regardless, the effective Hamiltonian for the sensor is \hat{G} , while θ acts analogously to time. Assuming the sensor is prepared in a pure state $|\psi\rangle$, the energy-time uncertainty principle

tells us that, the larger the variance $\langle \psi | (\Delta \hat{G})^2 | \psi \rangle$, the faster the sensor will evolve with respect to θ . So, the larger the variance $\langle \psi | (\Delta \hat{G})^2 | \psi \rangle$, the more responsive the sensor will be to small variations in θ . Indeed, the quantum Fisher information (QFI) [27] for this protocol, which quantifies the precision with which θ can be measured, is simply this variance $F_{\hat{G}}(|\psi\rangle) = \langle \psi | (\Delta \hat{G})^2 | \psi \rangle$.¹ From the first line of Eq. (1), we see that the ORT measure for pure states is based on the maximum quadrature variance — in other words, the Fisher information when using the sensor's optimal quadrature as the generator. Since the maximum quadrature variance of a coherent state is always $\frac{1}{2}$, $\mathcal{N}(|\alpha\rangle) = 0$ for coherent states $|\alpha\rangle$. For nonclassical states, the maximum quadrature variance is always greater than $\frac{1}{2}$, and $\mathcal{N} > 0$ describes the sensing enhancement over coherent states. We refer to this sensing enhancement as the *metrological power* \mathcal{W} [16, 18]. For pure states, $\mathcal{N}(|\psi\rangle) = \mathcal{W}(|\psi\rangle)$.

One may wonder why the ORT measure for pure states is based only on the maximum variance *quadrature*, as opposed to the maximum variance Hermitian generator \hat{G} in general (quadrature or not). This has to do with the resource-theoretic nature of the ORT measure. A unitary $e^{-i\theta\hat{X}_{\mu}}$ is a free operation for classical states [13, 16]—when it acts on a coherent state, it displaces it in phase space, yielding a new coherent state. Another free operator for evaluating nonclassicality is to use a phase shifter, i.e., $\hat{G} = \hat{a}^{\dagger}\hat{a}$. It is shown that the generator turns into an effective quadrature operator \hat{X}_{μ} in a multi-port phase sensing scheme with a single-mode nonclassical input in combination with classical light [18].

B. Mixed states

Before introducing the ORT measure for mixed states, one should first clarify what it means for a mixed state to be classical or nonclassical. A mixed bosonic state is defined as classical if and only if its density matrix $\hat{\rho}$ can be regarded as a classical mixture of coherent states. Otherwise, the state is considered nonclassical. Equivalently, one may determine if a state is classical by examining its Glauber-Sudarshan P -function. Any bosonic state $\hat{\rho}$ can be represented using its Glauber-Sudarshan P -function [28, 29] as

$$\hat{\rho} = \int P(\alpha, \alpha^*) |\alpha\rangle \langle \alpha| d^2\alpha. \quad (2)$$

The state $\hat{\rho}$ is defined as classical if $P(\alpha, \alpha^*)$ is positive semidefinite, in which case $P(\alpha, \alpha^*)$ acts as a classical probability density over the coherent states $|\alpha\rangle$. Otherwise, the state is nonclassical [30, 31].

¹ In this paper, we drop a factor of 4 from the standard definition of the QFI.

The ORT measure of nonclassicality for mixed states is:

$$\begin{aligned} \mathcal{N}(\hat{\rho}) &= \min_{\{q_j, |\phi_j\rangle\}} \left[\max_{\mu} \sum_j q_j \langle \phi_j | (\Delta \hat{X}_{\mu})^2 | \phi_j \rangle \right] - \frac{1}{2} \\ &= \min_{\{q_j, |\phi_j\rangle\}} \left[\sum_j q_j (\bar{n}_j - |\bar{\alpha}_j|^2) + \left| \sum_j q_j (\bar{\xi}_j - \bar{\alpha}_j^2) \right| \right]. \end{aligned} \quad (3)$$

Here, we have defined $\bar{n}_j \equiv \langle \phi_j | \hat{a}^{\dagger} \hat{a} | \phi_j \rangle$, $\bar{\alpha}_j \equiv \langle \phi_j | \hat{a} | \phi_j \rangle$, and $\bar{\xi}_j = \langle \phi_j | \hat{a}^2 | \phi_j \rangle$. The minimization is over all possible decompositions (ensembles) $\{q_j, |\phi_j\rangle\}$ of $\hat{\rho}$, satisfying $\hat{\rho} = \sum_j q_j |\phi_j\rangle \langle \phi_j|$ with $q_j > 0$. If $\hat{\rho}$ is mixed (i.e., $\text{rank}(\hat{\rho}) > 1$), then the number of states in a decomposition of $\hat{\rho}$ may be any number larger than $\text{rank}(\hat{\rho})$, making the calculation of $\mathcal{N}(\hat{\rho})$ a highly complex optimization problem in general, hence this paper.

The definition of $\mathcal{N}(\hat{\rho})$ satisfies several important conditions, as proved in Ref. [16]. (i) *Non-negativity*: $\mathcal{N}(\hat{\rho}) \geq 0$, where equality holds if and only if $\hat{\rho}$ is classical. Non-negativity is the minimum requirement for a nonclassicality measure. (ii) *Weak monotonicity*: \mathcal{N} cannot increase under any classical operation Λ : $\mathcal{N}(\Lambda[\hat{\rho}]) \leq \mathcal{N}(\hat{\rho})$. A classical operation is an operation that cannot create superpositions of coherent states from mixtures of coherent states (such as the use of passive linear optical operations and displacements). For details, see Ref. [16, 17]. Weak-monotonicity makes the ORT measure resource-theoretic; classical operations are the free operations of the resource theory. (iii) *Convexity*: $\sum_j p_j \mathcal{N}(\hat{\rho}_j) \geq \mathcal{N}(\sum_j p_j \hat{\rho}_j)$ for any quantum states $\hat{\rho}_j$ and probabilities p_j . (iv) *Lower-bounded by metrological power*: $\mathcal{N}(\hat{\rho}) \geq \mathcal{W}(\hat{\rho})$, where equality holds for pure states. The metrological power for mixed states is defined as $\mathcal{W}(\hat{\rho}) \equiv \max[F_X(\hat{\rho}) - 1/2, 0]$, where [16, 17]

$$F_X(\hat{\rho}) = \max_{\mu} \left[\min_{\{q_j, |\phi_j\rangle\}} \left(\sum_j q_j \langle \phi_j | (\Delta \hat{X}_{\mu})^2 | \phi_j \rangle \right) \right] \quad (4)$$

is the QFI for the optimal quadrature angle. Notice that for mixed states, the QFI also involves a minimization over all possible ensembles (and maximization over quadratures), although the order of the maximization and minimization in Eq. (3) and (4) makes a subtle yet important difference (in fact, the QFI can be computed given an eigenstate decomposition of $\hat{\rho}$ [32]). Again, the metrological power \mathcal{W} describes the sensing enhancement over classical states: for all classical states, $\mathcal{W} = 0$. Notably, there exist nonclassical mixed states for which $\mathcal{W} = 0$ [16, 17]. Thus, the tight inequality $\mathcal{N}(\hat{\rho}) \geq \mathcal{W}(\hat{\rho})$ is the closest possible relationship between a resource-theoretic nonclassicality measure and the metrological power.

III. METHOD

The ORT measure for mixed states, Eq. (3), is an example of a *convex roof construction*. Such constructions commonly arise in other nonclassicality measures [11, 14, 15], as well as entanglement measures, for mixed states [25, 26].

Evaluating the convex roof is a matter of optimizing an objective function over the set of all convex decompositions of a state $\hat{\rho}$. Optimizing the objective function is a challenging problem, a primary difficulty being that the number of states in a decomposition of a mixed state may be any number larger than its rank, although some clever techniques that bound or approximate the answer have been proposed [25, 33].

Rather than adapt previous techniques to our problem, here we introduce a new method based on linear programming. Our method is similar to variational methods for ground state energy calculations, in that we essentially make a variational ansatz over the space of decompositions. It has the pedagogical advantage that it is highly intuitive and easy to employ.

A. Fock-diagonal states

In particular, we utilize our method to evaluate the ORT measure for mixed states that are diagonal in the Fock basis: $\hat{\rho} = \sum_n p_n |n\rangle \langle n|$, where $|n\rangle$ is the Fock state with photon number n and $\{p_n, |n\rangle\}$ is one possible decomposition. Such states arise often due to dephasing effects [22–24], which eliminate the coherence between different Fock states. We refer to the probabilities p_n as *populations*. For such states, the ORT measure simplifies to:

$$\begin{aligned} \mathcal{N}(\hat{\rho}) &= \langle \hat{a}^{\dagger} \hat{a} \rangle - \max_{\{q_j, |\phi_j\rangle\}} \left(\sum_j q_j |\bar{\alpha}_j|^2 - \left| \sum_j q_j \bar{\alpha}_j^2 \right| \right) \\ &\leq \langle \hat{a}^{\dagger} \hat{a} \rangle. \end{aligned} \quad (5)$$

The inequality is saturated by states in which all nonzero populations have associated photon numbers that differ by at least 2 from one another [17]. An example is $p|0\rangle \langle 0| + (1-p)|2\rangle \langle 2|$, whose population constraints imply that any decomposition state has the form $|\phi_j\rangle = |0\rangle \langle 0| \phi_j\rangle + |2\rangle \langle 2| \phi_j\rangle$ — it follows that $\alpha_j = \langle \phi_j | \hat{a} | \phi_j \rangle = 0$ for all $|\phi_j\rangle$. It is thus more worthwhile to evaluate the ORT measure for Fock-diagonal states where *neighboring* photon numbers have nonzero populations.

Prior ORT measure calculations [17] only addressed Fock-diagonal states with *two* neighboring populations: $\hat{\rho}_{2F} = p_{n+1} |n+1\rangle \langle n+1| + (1-p_{n+1}) |n\rangle \langle n|$. It was found that the optimal decomposition for such states was a “four-prong” set of superposition states: $|\phi_j\rangle = \sqrt{p_{n+1}} |n+1\rangle + \sqrt{1-p_{n+1}} e^{ij\pi/2} |n\rangle$ with equal weights

$q_j = 1/4$ ($j = 0, 1, 2, 3$).² The phases $e^{ij\pi/2}$, which are the quartic roots of unity, cause $\sum_j q_j \bar{\alpha}_j^2 = 0$ — thus the absolute value term in Eq. (5) vanishes with this decomposition. Plugging this decomposition into Eq. (5) gives: $\mathcal{N}(\hat{\rho}_{2F}) = n + p_{n+1} - (n+1)p_{n+1}(1 - p_{n+1})$.³ This result serves as a basic check of our method, and provides some insight into the types of optimal decompositions one may expect in more complicated cases.

B. Linear-programming method

Now we will describe our method for calculating the ORT measure. For simplicity, we will first explain it in the context of calculating $\mathcal{N}(\hat{\rho}_{2F})$. Then we will explain how to apply the method to Fock-diagonal states with more nonzero populations.

Any state occurring in a decomposition of $\hat{\rho}$ must be in the support of $\hat{\rho}$. Thus, for $\hat{\rho}_{2F}$, each decomposition state must be of the form $|\phi(x, \theta)\rangle = x|n+1\rangle + \sqrt{1-x^2}e^{i\theta}|n\rangle$, where $x \in [0, 1]$ and $\theta \in [0, 2\pi]$. Just as there are infinitely many decompositions of $\hat{\rho}_{2F}$, there are infinitely many probability distributions $q(x, \theta)$ such that $\int_0^1 dx \int_0^{2\pi} d\theta q(x, \theta) |\phi(x, \theta)\rangle \langle \phi(x, \theta)| = \hat{\rho}_{2F}$. We prefer to think of the problem of finding the optimal decomposition as a problem of finding the optimal probability distribution $q(x, \theta)$. Each $q(x, \theta)$ satisfies the constraints:

$$\int_0^1 dx \int_0^{2\pi} d\theta q(x, \theta) = 1 \quad (6)$$

$$\int_0^1 dx \int_0^{2\pi} d\theta x^2 q(x, \theta) = p_{n+1} \quad (7)$$

$$\int_0^1 dx \int_0^{2\pi} d\theta x \sqrt{1-x^2} e^{i\theta} q(x, \theta) = 0 \quad (8)$$

$$q(x, \theta) \geq 0. \quad (9)$$

Respectively, the above constraints address normalization, population constraints, lack of off-diagonal elements, and positivity of all contributions (i.e., that the distribution describes a convex combination of states). Although we express $q(x, \theta)$ as if it were a continuous probability distribution here, the optimal distribution (decomposition) may be discrete. In terms of $q(x, \theta)$,

Eq. (3) reads:

$$\mathcal{N}(\hat{\rho}_{2F}) - \langle \hat{a}^\dagger \hat{a} \rangle = - \max_{q(x, \theta)} \left(\int_0^1 dx \int_0^{2\pi} d\theta q(x, \theta) |\bar{\alpha}_{x, \theta}|^2 - \left| \int_0^1 dx \int_0^{2\pi} d\theta q(x, \theta) \bar{\alpha}_{x, \theta}^2 \right| \right) \quad (10)$$

where $\bar{\alpha}_{x, \theta} = x\sqrt{1-x^2}\sqrt{n+1}e^{-i\theta}$. The quantity to be maximized on the right hand side of 10 is called the objective function $\mathcal{L}[q(x, \theta)]$:

$$\mathcal{L}[q(x, \theta)] = \int_0^1 dx \int_0^{2\pi} d\theta q(x, \theta) |\bar{\alpha}_{x, \theta}|^2 - \left| \int_0^1 dx \int_0^{2\pi} d\theta q(x, \theta) \bar{\alpha}_{x, \theta}^2 \right|. \quad (11)$$

The second term in the objective function may appear problematic, due to the absolute value. However, without loss of generality, it can be taken to vanish (for our class of states). This is because, given any $q(x, \theta)$, it is always possible to find a distribution $\tilde{q}(x, \theta)$ such that $\mathcal{L}[\tilde{q}(x, \theta)] \geq \mathcal{L}[q(x, \theta)]$ and $\int_0^1 dx \int_0^{2\pi} d\theta \tilde{q}(x, \theta) \bar{\alpha}_{x, \theta}^2 = 0$. The idea is to reallocate the probability from $q(x, \theta)$ in a four-prong formation for each x : $\tilde{q}(x, \theta) = \frac{1}{4} \left(\int_0^{2\pi} d\theta' q(x, \theta') \right) \left(\sum_{j=0}^3 \delta(\theta - \theta_0 - \frac{j\pi}{2}) \right)$, where $\theta_0 \in (0, 2\pi)$ is arbitrary. It is straightforward to check that $\tilde{q}(x, \theta)$ satisfies the same constraints (Eq. (6)-(9)) as the $q(x, \theta)$ from which it was constructed; meanwhile, it causes the absolute term in the objective function \mathcal{L} to vanish, while maintaining the value of the remaining term.

Since the θ -dependence of $\tilde{q}(x, \theta)$ is removed, we may rename it $\mathcal{Q}(x) \equiv \tilde{q}(x, \theta)$. For our purposes, it is sufficient to optimize the x -dependence of $\mathcal{Q}(x)$, subject to the constraints $\int_0^1 dx \mathcal{Q}(x) = 1$, $\int_0^1 dx x^2 \mathcal{Q}(x) = p_{n+1}$, and $\mathcal{Q}(x) \geq 0$. In terms of $\mathcal{Q}(x)$, Eq. (10) becomes:

$$\mathcal{N}(\hat{\rho}_{2F}) - \langle \hat{a}^\dagger \hat{a} \rangle = - \max_{\mathcal{Q}(x)} \left(\int_0^1 dx \mathcal{Q}(x) x^2 (1-x^2)(n+1) \right). \quad (12)$$

The optimization problem (including constraints) resembles a *linear programming* problem [34] for the vector $\mathcal{Q}(x)$, the only caveat being that $\mathcal{Q}(x)$ does not have a discrete number of components. Nevertheless, the solution to the problem can be approximated by discretizing the set of possible x (i.e., binning):

$$- \max_{\mathcal{Q}_x} \left(\sum_{x \in \mathcal{X}} \mathcal{Q}_x x^2 (1-x^2)(n+1) \right) \gtrsim \mathcal{N}(\hat{\rho}_{2F}) - \langle \hat{a}^\dagger \hat{a} \rangle \quad (13)$$

² Actually, there are multiple optimal decompositions (for example a “three-prong set” with relative phases that are the cubic roots of unity), but they share the property that $|\langle n+1 | \phi_j \rangle| = \sqrt{p_{n+1}}$ for all $|\phi_j\rangle$.

³ That this value is optimal may be further justified via its convexity as a function of p_{n+1} .

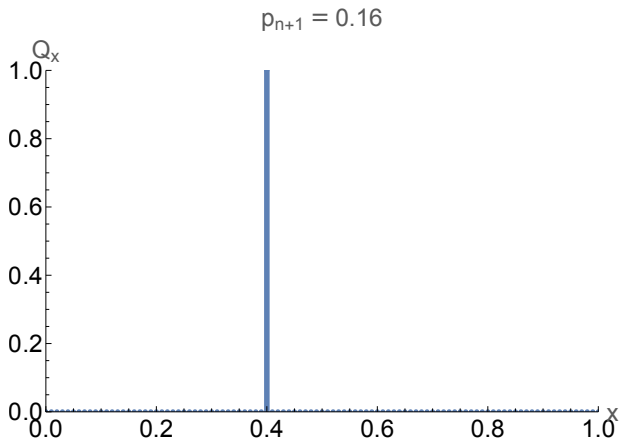


FIG. 1. Optimal discrete probability distribution \mathcal{Q}_x for $\hat{\rho}_{2F} = 0.16 |n+1\rangle \langle n+1| + 0.84 |n\rangle \langle n|$ (the value of n has no effect here). The spacing between x bins is $\Delta = 0.01$. One may notice that $\mathcal{Q}_{\sqrt{p_{n+1}}} = 1$ and $\mathcal{Q}_x = 0$ for all other x , thus reproducing the expected result from Ref. [17].

$$\sum_{x \in \mathcal{X}} \mathcal{Q}_x = 1 \quad (14)$$

$$\sum_{x \in \mathcal{X}} x^2 \mathcal{Q}_x = p_{n+1} \quad (15)$$

$$\mathcal{Q}_x \geq 0. \quad (16)$$

Here, \mathcal{X} is a discrete set of points in the range $[0, 1]$. In this work, we take \mathcal{X} to be the set of real numbers $m\Delta \leq 1$, where m is a non-negative integer and Δ is the spacing of the binning with $0 < \Delta \ll 1$. The approximation, Eq. (13), should converge as $\Delta \rightarrow 0$ (here \gtrsim means approximately equal to, but never less than).

Here \mathcal{Q}_x is a discrete probability distribution (“histogram”) over the set of points in \mathcal{X} . As such, it is essentially a variational ansatz for the optimal decomposition, which can be optimized by linear programming. We solve the linear program using the LINEAROPTIMIZATION function in MATHEMATICA. An example is demonstrated in Fig. 1. \mathcal{Q}_x is spiked at $x = \sqrt{p_{n+1}}$ and zero elsewhere. This holds for all choices of p_{n+1} (though one should be mindful and bin appropriately in the extremes $p_{n+1} \ll 1$ and $1 - p_{n+1} \ll 1$). Thus, the optimal decomposition utilizes the four-prong set of states $|\phi_j\rangle = \sqrt{p_{n+1}} |n+1\rangle + \sqrt{1-p_{n+1}} e^{i(j\pi/2 + \theta_0)}$ (where $j = 0, 1, 2, 3$), with probability 1/4 for each. This corroborates our method, since it reproduces the results of Ref. [17].

Note that, due to a careful choice of parameters (and binning) for Fig. 1, the discrete distribution matches the true optimal decomposition perfectly. This will not always be the case (generally, the discrete distribution will be slightly suboptimal, acting as a bound). However, one can work backwards from the numerical evidence to conjecture the true optimal decomposition (i.e. realize that $0.4 = \sqrt{0.16}$, in Fig. 1). The conjecture of the ansatz can then be corroborated by checking it against

finer binnings. In this way, we obtain analytic expressions for $\mathcal{N}(\hat{\rho}_{3F})$ and $\mathcal{N}(\hat{\rho}_{4F})$, in section IV.

C. Higher-rank Fock-diagonal states

A more general Fock-diagonal state, with neighboring populations, is:

$$\hat{\rho}_{MF} = \sum_{k=0}^{M-1} p_{n+k} |n+k\rangle \langle n+k|. \quad (17)$$

Any decomposition state for $\hat{\rho}_{MF}$ must be of the form:

$$|\phi(\vec{x}, \vec{\theta})\rangle = \sum_{k=0}^{M-1} x_k e^{i\theta_k} |n+k\rangle, \quad (18)$$

where $x_k \in [0, 1]$, $\theta_k \in [0, 2\pi]$, and $\sum_k x_k^2 = 1$. Without loss of generality, one can take $\theta_{M-1} = 0$, and $x_0 = \sqrt{1 - \sum_{k=1}^{M-1} x_k^2}$. $\hat{\rho}_{MF}$ may then be expressed as a summation over these states with probabilities $q(\vec{x}, \vec{\theta})$ satisfying certain constraints. The nonclassicality calculation then becomes a matter of optimizing $q(\vec{x}, \vec{\theta})$. Similar to the case of $\hat{\rho}_{2F}$, it is sufficient to optimize a probability distribution $\mathcal{Q}(\vec{x})$ over the amplitudes x_k with symmetric $\vec{\theta}$ -dependence. The optimization problem can be solved approximately by discretizing the set of possible \vec{x} :

$$-\max_{\mathcal{Q}_{\vec{x}}} \left(\sum_{\vec{x} \in \mathcal{X}} \mathcal{Q}_{\vec{x}} \left(\sum_{k=0}^{M-2} x_{k+1} x_k \sqrt{n+k+1} \right)^2 \right) \gtrsim \mathcal{N}(\hat{\rho}_{MF}) - \langle \hat{a}^\dagger \hat{a} \rangle \quad (19)$$

$$\sum_{\vec{x} \in \mathcal{X}} \mathcal{Q}_{\vec{x}} = 1 \quad (20)$$

$$\sum_{\vec{x} \in \mathcal{X}} x_k^2 \mathcal{Q}_{\vec{x}} = p_{n+k} \quad (21)$$

$$\mathcal{Q}_{\vec{x}} \geq 0. \quad (22)$$

In this work, we take $(x_1, x_2, \dots, x_{M-1}) = (l_1\Delta, l_2\Delta, \dots, l_{M-1}\Delta)$, where $\sum_{k=1}^{M-1} l_k^2 \Delta^2 \leq 1$, the l_k are non-negative integers, and $0 < \Delta \ll 1$. The approximation, Eq. (19) should converge as $\Delta \rightarrow 0$. Note that $\mathcal{Q}_{\vec{x}}$ is essentially a vector in \mathbb{R}^d , where d is the number of elements in \mathcal{X} . For fixed Δ , d scales as Δ^{-M+1} . The optimization may be carried out using linear programming, as before, although the computational complexity will increase with M .

Note that an upper bound on the ORT measure can easily be found by plugging in the simple decomposition $\mathcal{Q}_{\vec{x}} = \prod_{k=1}^{M-1} \delta_{x_k, \sqrt{p_k}}$:

$$\mathcal{N}(\hat{\rho}_{MF}) \leq \langle \hat{a}^\dagger \hat{a} \rangle - \left(\sum_{k=0}^{M-2} \sqrt{p_{k+1} p_k (n+k+1)} \right)^2. \quad (23)$$

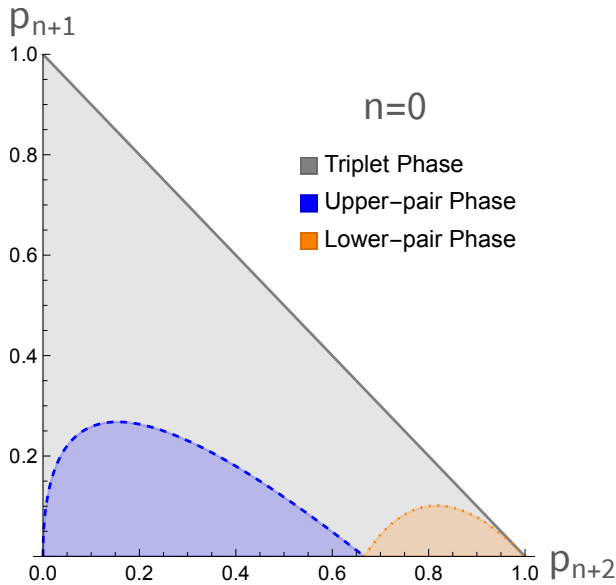


FIG. 2. Phase space for $\hat{\rho}_{3F}$ assuming the lowest populated photon number is $n = 0$. The expression for the ORT measure $\mathcal{N}(\hat{\rho}_{3F})$ depends on which of three distinct phases the state is in (although $\mathcal{N}(\hat{\rho}_{3F})$ is still piecewise continuous as shown in Fig. 3). These phases are named according to what their optimal decompositions look like. For $n > 0$, the general shape of these phases is maintained, although the point where the curves intersect the bottom axis shifts left as $p_{n+2} = \frac{2+n}{3+2n}$.

Equality holds in the $M = 2$ case (where this simple decomposition is optimal), as demonstrated previously. For $M > 2$, we find (see section IV) that equality holds in some regimes (i.e., some choices of the populations p_k), but not all.

IV. NUMERICAL RESULTS AND ANALYTICAL ANSATZ

A. Rank-3 case

For fixed n in $\hat{\rho}_{3F} = p_{n+2} |n+2\rangle \langle n+2| + p_{n+1} |n+1\rangle \langle n+1| + (1 - p_{n+2} - p_{n+1}) |n\rangle \langle n|$, there are two free parameters: p_{n+2} and p_{n+1} . The possible choices (p_{n+2}, p_{n+1}) of these parameters form the 45-45-90 triangle defined by $p_{n+2} + p_{n+1} \leq 1$, $p_{n+2} \geq 0$, and $p_{n+1} \geq 0$. From our numerical investigations, we deduced that there are three distinct regimes, or *phases*, within this triangular phase space (see Fig. 2).

1. Triplet phase

In Fig. 2, the triplet phase is the upper, gray regime (the lower boundary of which is given in ensuing subsections). Each state in the optimal decomposition of $\hat{\rho}_{3F}$

is of the form:

$$|\phi_T(\theta_j, \gamma_j)\rangle = \sqrt{p_{n+2}} |n+2\rangle + \sqrt{p_{n+1}} e^{i\theta_j} |n+1\rangle + \sqrt{1 - p_{n+2} - p_{n+1}} e^{i\gamma_j} |n\rangle. \quad (24)$$

As stated before, the decomposition states come in a four-prong set ($j = 0, 1, 2, 3$) with equal weights and the relative phases θ_j and γ_j is determined by the choice of the phase of the coherence α_j . For context, this decomposition is a straightforward generalization of the optimal decomposition for density matrices that are diagonal in *two* neighboring Fock states, $\hat{\rho}_{2F} = p_{n+1} |n+1\rangle \langle n+1| + p_n |n\rangle \langle n|$ (see section III and [17]). The ORT measure for states in this regime is:

$$\mathcal{N}(\hat{\rho}_{3F}) = 2p_{n+2} + p_{n+1} + n - \left(\sqrt{p_{n+2}} \sqrt{n+2} + \sqrt{1 - p_{n+2} - p_{n+1}} \sqrt{n+1} \right)^2 p_{n+1}. \quad (25)$$

In this case, the bound in Eq. (23) is saturated.

What stands out about this decomposition is the fact that $|\langle n+2 | \phi_T(\theta_j, \gamma_j) \rangle|^2 = p_{n+2}$, $|\langle n+1 | \phi_T(\theta_j, \gamma_j) \rangle|^2 = p_{n+1}$, and $|\langle n | \phi_T(\theta_j, \gamma_j) \rangle|^2 = 1 - p_{n+2} - p_{n+1}$. We call this decomposition the “triplet” decomposition (and the phase where it is optimal the triplet phase) because of this symmetric treatment of the three photon numbers.

Of course, it is always possible to decompose $\hat{\rho}_{3F} = p_{n+2} |n+2\rangle \langle n+2| + p_{n+1} |n+1\rangle \langle n+1| + p_n |n\rangle \langle n|$ into the four states $|\phi_T(\theta_j, \gamma_j)\rangle$. However, it turns out that the triplet decomposition is *not* optimal for all choices of (p_{n+2}, p_{n+1}) . For some values of (p_{n+2}, p_{n+1}) , a more optimal decomposition is possible.

2. Upper-pair phase

In Fig. 2, the upper-pair phase is the lower-left, blue regime. Five states are a part of the optimal decomposition of $\hat{\rho}_{3F}$. One is the Fock state $|n\rangle$. The other four states are of the form:

$$|\phi_U(\theta_j, \gamma_j)\rangle = \sqrt{1-f} e^{i\gamma_j} |n\rangle + \sqrt{f} \left(\sqrt{\frac{p_{n+2}}{p_{n+2} + p_{n+1}}} |n+2\rangle + \sqrt{\frac{p_{n+1}}{p_{n+2} + p_{n+1}}} e^{i\theta_j} |n+1\rangle \right), \quad (26)$$

where:

$$f = \frac{(2+n)p_{n+2}}{(1+n)p_{n+1} + (3+2n)p_{n+2}}. \quad (27)$$

The states $|\phi_U(\theta_j, \gamma_j)\rangle$ contribute a total probability $(p_{n+2} + p_{n+1}) f^{-1}$ (each contributes 1/4 of this). The ORT measure is:

$$\mathcal{N}(\hat{\rho}_{3F}) = 2p_{n+2} + p_{n+1} + n - (p_{n+2} + p_{n+1}) f^{-1} |\langle \phi_U(0,0) | \hat{a} | \phi_U(0,0) \rangle|^2. \quad (28)$$

What stands out about this decomposition is the fact that $|\langle n+2|\phi_U(\theta_j, \gamma_j)\rangle|^2 / |\langle n+1|\phi_U(\theta_j, \gamma_j)\rangle|^2 = p_{n+2}/p_{n+1}$, the population ratio between $|n+2\rangle$ and $|n+1\rangle$ in the original density matrix $\hat{\rho}_{3F}$. By contrast, $|\langle n|\phi_U(\theta_j, \gamma_j)\rangle|^2$ does not have a neat connection to the population ratios in the original density matrix. Moreover, $|n\rangle$ is also a state in the optimal decomposition. Due to this asymmetric treatment of the photon numbers, we call this the upper-pair phase.

One may wonder how the value of f was obtained, given its unintuitive appearance. First, we deduced from the linear optimization that, for some values of (p_{n+2}, p_{n+1}) , the optimal decomposition involved the Fock state $|n\rangle$ and states of the form $|\phi_U(\theta_j, \gamma_j)\rangle$ (see Eq. (26)). We then optimized the value of f in Eq. (26) analytically, yielding Eq. (27).

Such a decomposition is not possible everywhere, though. As previously mentioned, the states $|\phi_U(\theta_j, \gamma_j)\rangle$ contribute a total probability $(p_{n+2} + p_{n+1})f^{-1}$. This cannot exceed 1. Thus:

$$p_{n+2} + p_{n+1} \leq \frac{(2+n)p_{n+2}}{(1+n)p_{n+1} + (3+2n)p_{n+2}}. \quad (29)$$

This sets the upper bound on this phase (blue dashed curve in Fig. 2): note that, at the upper bound, $|\phi_U(\theta_j, \gamma_j)\rangle = |\phi_T(\theta_j, \gamma_j)\rangle$. To find the highest possible value of p_{n+2} , we can set $p_{n+1} = 0$ and saturate the inequality:

$$p_{n+2}^{\max} = \frac{2+n}{3+2n}. \quad (30)$$

3. Lower-pair phase

In Fig. 2, the lower-pair phase is the lower-right, orange regime. It is analogous to the upper-pair phase, except that in the optimal decomposition it is the lower-two Fock states $|n+1\rangle$ and $|n\rangle$ that are ‘‘paired.’’ Five states are a part of the optimal decomposition of $\hat{\rho}_{3F}$. One is the Fock state $|n+2\rangle$. The other four are states of the form:

$$\begin{aligned} |\phi_L(\theta_j, \gamma_j)\rangle &= \sqrt{1-g}|n+2\rangle \\ &+ \sqrt{g} \left(\sqrt{\frac{p_{n+1}}{1-p_{n+2}}} e^{i\theta_j} |n+1\rangle + \sqrt{\frac{1-p_{n+2}-p_{n+1}}{1-p_{n+2}}} e^{i\gamma_j} |n\rangle \right), \end{aligned} \quad (31)$$

where:

$$g = \frac{(1+n)(-1+p_{n+1}+p_{n+2})}{-3-2n+(1+n)p_{n+1}+(3+2n)p_{n+2}}. \quad (32)$$

The states $|\phi_L(\theta_j, \gamma_j)\rangle$ contribute a total probability $(1-p_{n+2})g^{-1}$ (each contributes 1/4 of this). The ORT measure is:

$$\begin{aligned} \mathcal{N}(\hat{\rho}_{3F}) &= 2p_{n+2} + p_{n+1} + n \\ &- (1-p_{n+2})g^{-1} |\langle \phi_L(0,0) | \hat{a} | \phi_L(0,0) \rangle|^2. \end{aligned} \quad (33)$$

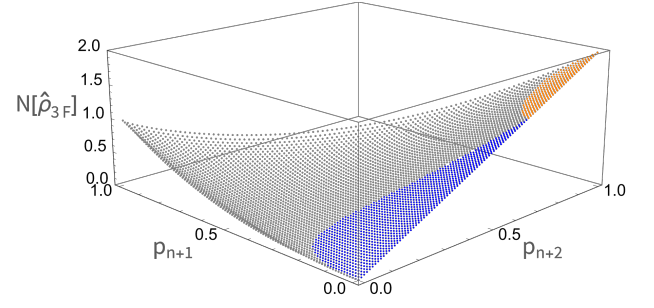


FIG. 3. Nonclassicality $\mathcal{N}(\hat{\rho}_{3F})$ over the entire phase space of $\hat{\rho}_{3F}$. Here, the lowest populated photon number is assumed to be $n=0$. At the corners, which represent Fock states, the nonclassicality takes the values 0, 1, and 2. The nonclassicality is continuous despite there being three distinct phases (see Fig. 2). The points in each phase are colored differently here for reference.

We call this the ‘‘lower-pair phase’’ due to the asymmetric treatment of the photon numbers. $|\langle n+1|\phi_L(\theta_j, \gamma_j)\rangle|^2 / |\langle n|\phi_L(\theta_j, \gamma_j)\rangle|^2 = p_{n+1}/(1-p_{n+2}-p_{n+1})$, the population ratio between $|n+1\rangle$ and $|n\rangle$ in the original state. By contrast, $|\langle n+2|\phi_L(\theta_j, \gamma_j)\rangle|^2$ does not have a simple connection to the population ratios in the original density matrix; also, $|n+2\rangle$ is itself a state in the optimal decomposition.

The value of g was obtained in the same way that f in Eq. (27) was. We deduced from the linear optimization that, for some values of (p_{n+2}, p_{n+1}) , the optimal decomposition involved the Fock state $|n+2\rangle$ and states of the form $|\phi_L(\theta_j, \gamma_j)\rangle$ (see Eq. (31)). We then optimized g in Eq. (31) analytically.

Similarly, the total probability $(1-p_{n+2})g^{-1}$ contributed by the states $|\phi_L(\theta_j, \gamma_j)\rangle$ cannot exceed 1 such that

$$1-p_{n+2} \leq \frac{(1+n)(-1+p_{n+1}+p_{n+2})}{-3-2n+(1+n)p_{n+1}+(3+2n)p_{n+2}}. \quad (34)$$

This sets the upper bound on this phase (orange dotted curve in Fig. 2): note that, at the upper bound, $|\phi_L(\theta_j, \gamma_j)\rangle = |\phi_T(\theta_j, \gamma_j)\rangle$. To find the lowest possible value of p_{n+2} , we can set $p_{n+1} = 0$ and saturate the inequality:

$$p_{n+2}^{\min} = \frac{2+n}{3+2n}. \quad (35)$$

Having scanned over various values of (p_{n+2}, p_{n+1}) , and numerically approximated $\mathcal{N}(\hat{\rho}_{3F})$ for each, we are reasonably confident (although we lack analytical proof) that these three phases (triplet, upper-pair, and lower-pair) are the only three, and that we have characterized the nonclassicality exactly over the entire phase space of $\hat{\rho}_{3F}$. Assuming the ansatz, the nonclassicality is plotted in Fig. 3

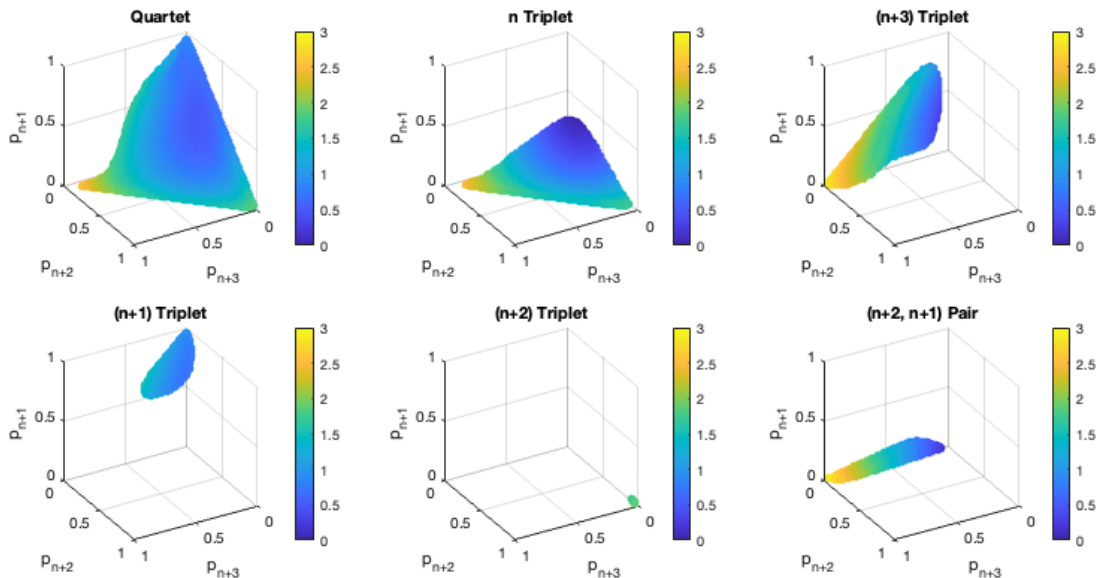


FIG. 4. Nonclassicality $\mathcal{N}(\hat{\rho}_{4F})$ over the phase space of $\hat{\rho}_{4F}$, assuming the lowest populated photon number of $n = 0$. To our knowledge, there are six distinct regimes (phases), in which there are distinct ways of optimally decomposing $\hat{\rho}_{4F}$. The complete phase space composed of these regimes is the triangular pyramid defined by $p_{n+3} + p_{n+2} + p_{n+1} \leq 1$. This plot was created by calculating the ORT measure at discrete points within each phase, and some phases may be larger than they appear. At the vertices of the pyramid (which represent Fock states), the ORT measure takes the values 0, 1, 2, and 3.

B. Rank-4 case

For fixed n in $\hat{\rho}_{4F} = p_{n+3}|n+3\rangle\langle n+3| + p_{n+2}|n+2\rangle\langle n+2| + p_{n+1}|n+1\rangle\langle n+1| + (1 - p_{n+3} - p_{n+2} - p_{n+1})|n\rangle\langle n|$, there are three free param-

eters: p_{n+3} , p_{n+2} , and p_{n+1} . The possible choices $(p_{n+3}, p_{n+2}, p_{n+1})$ of these parameters form the triangular pyramid defined by $p_{n+3} + p_{n+2} + p_{n+1} \leq 1$, $p_{n+3} \geq 0$, $p_{n+2} \geq 0$, and $p_{n+1} \geq 0$. From our numerical investigations, we found six distinct regimes, or phases, within this pyramidal phase space. These fall into three categories: which we call *quartet*, *triplet*, and *pair*.

1. Quartet Phase

The quartet phase is shown in Fig. 4 (upper-left). This phase comprises the majority of the phase space, in the same way that the triplet phase comprises the majority of the phase space in the rank-3 case. This phase has the most simple optimal decomposition, utilizing states of the form:

$$|\phi_Q(\theta_j, \gamma_j, \zeta_j)\rangle = \sqrt{p_{n+3}}|n+3\rangle + \sqrt{p_{n+2}}e^{i\theta_j}|n+2\rangle + \sqrt{p_{n+1}}e^{i\gamma_j}|n+1\rangle + \sqrt{p_n}e^{i\zeta_j}|n\rangle, \quad (36)$$

where $p_n = 1 - \sum_{k=1}^3 p_{n+k}$. These states are a straightforward generalization of the states in Eq. (24). As before, the decomposition states come in a symmetric set with equal weights. We call this the quartet phase because all four photon numbers are treated symmetrically, with amplitudes equal to the square root of the populations. The ORT measure for states in this regime

is:

$$\mathcal{N}(\hat{\rho}_{4F}) = 3p_{n+3} + 2p_{n+2} + p_{n+1} + n - \left(\sum_{k=0}^2 \sqrt{p_{n+k+1}p_{n+k}(n+k+1)} \right)^2. \quad (37)$$

In this case, the bound in Eq. (23) is saturated.

It is always possible to decompose $\hat{\rho}_{4F}$ into the states in Eq. (36). However, this decomposition is not optimal for all choices of $(p_{n+3}, p_{n+2}, p_{n+1})$. The regions where the quartet decomposition is not optimal (and, consequently, the boundaries of the quartet phase) are described in the following.

2. Triplet Phases

The triplet phases are natural generalizations of the pair phases in the rank-3 case. There are four triplet

phases: the n -triplet, $(n+1)$ -triplet, $(n+2)$ -triplet, and $(n+3)$ -triplet.

n-triplet—The n -triplet phase is shown in the upper-middle panel of Fig. 4. The optimal decomposition consists of one Fock state, $|n\rangle$, as well as states of the form:

$$|\phi_{0T}(\theta_j, \gamma_j, \zeta_j)\rangle = \sqrt{1-f_0}e^{i\zeta_j}|n\rangle + \sqrt{f_0}\left(\sqrt{\frac{p_{n+3}}{1-p_n}}|n+3\rangle + \sqrt{\frac{p_{n+2}}{1-p_n}}e^{i\theta_j}|n+2\rangle + \sqrt{\frac{p_{n+1}}{1-p_n}}e^{i\gamma_j}|n+1\rangle\right). \quad (38)$$

Such states contribute a total probability $(1-p_n)f_0^{-1}$, which cannot exceed 1, and so $1 \geq f_0 \geq 1-p_n$. Here, f_0 is chosen to maximize the objective, i.e., make $(1-p_n)f_0^{-1}|\langle\phi_{0T}(0,0,0)|\hat{a}|\phi_{0T}(0,0,0)\rangle|^2$ as large as possible. f_0 is a quite complicated function of n and the populations, so we do not show its algebraic form here. The ORT measure for states in this phase is:

$$\mathcal{N}(\hat{\rho}_{4F}) = 3p_{n+3} + 2p_{n+2} + p_{n+1} + n - (1-p_n)f_0^{-1}|\langle\phi_{0T}(0,0,0)|\hat{a}|\phi_{0T}(0,0,0)\rangle|^2. \quad (39)$$

$f_0 = 1-p_n$ determines a boundary on this phase: note that $|\phi_{0T}(\theta_j, \gamma_j, \zeta_j)\rangle \rightarrow |\phi_Q(\theta_j, \gamma_j, \zeta_j)\rangle$ as $1-p_n \rightarrow f_0$. Interestingly, this condition is not sufficient to determine the entire boundary of this phase, because there are points $(p_{n+3}, p_{n+2}, p_{n+1})$ satisfying $f_0 \geq 1-p_n$ for which an even better decomposition exists, hence the $(n+2, n+1)$ -pair phase (see lower right panel of Fig. 4). Ultimately, the n -triplet phase consists of the points satisfying $f_0 \geq 1-p_n$ that are not part of the $(n+2, n+1)$ -pair phase.

Lastly, it is worth noting that the $p_{n+3} = 0$ face of the pyramidal phase space of $\hat{\rho}_{4F}$ corresponds to the rank-3 case with populated photon numbers $n+2$, $n+1$, and n ; the n -triplet phase is a smooth extension of the upper-pair phase on this rank-3 face.

(n+3)-triplet—The $(n+3)$ -triplet phase is shown in the upper-right panel of Fig. 4. The optimal decomposition consists of one Fock state, $|n+3\rangle$, as well as states of the form:

$$|\phi_{3T}(\theta_j, \gamma_j, \zeta_j)\rangle = \sqrt{1-f_3}|n+3\rangle + \sqrt{f_3}\left(\sqrt{\frac{p_{n+2}}{1-p_{n+3}}}e^{i\theta_j}|n+2\rangle + \sqrt{\frac{p_{n+1}}{1-p_{n+3}}}e^{i\gamma_j}|n+1\rangle + \sqrt{\frac{p_n}{1-p_{n+3}}}e^{i\zeta_j}|n\rangle\right). \quad (40)$$

Such states contribute a total probability $(1-p_{n+3})f_3^{-1}$, which cannot exceed 1, and so $1 \geq f_3 \geq 1-p_{n+3}$. Here, f_3 is chosen to maximize the objective, i.e., make $(1-p_{n+3})f_3^{-1}|\langle\phi_{3T}(0,0,0)|\hat{a}|\phi_{3T}(0,0,0)\rangle|^2$ as large as possible. Since f_3 is a quite complicated function of n and the populations, we do not show its algebraic form

here. The ORT measure for states in this phase is:

$$\mathcal{N}(\hat{\rho}_{4F}) = 3p_{n+3} + 2p_{n+2} + p_{n+1} + n - (1-p_{n+3})f_3^{-1}|\langle\phi_{3T}(0,0,0)|\hat{a}|\phi_{3T}(0,0,0)\rangle|^2. \quad (41)$$

$f_3 = 1-p_{n+3}$ determines a boundary on this phase: note that $|\phi_{3T}(\theta_j, \gamma_j, \zeta_j)\rangle \rightarrow |\phi_Q(\theta_j, \gamma_j, \zeta_j)\rangle$ as $1-p_{n+3} \rightarrow f_3$. This condition, however, is not sufficient to determine the entire boundary of this phase, because there are points $(p_{n+3}, p_{n+2}, p_{n+1})$ satisfying $f_3 \geq 1-p_{n+3}$ for which an even better decomposition exists (such points belong to the $(n+2, n+1)$ -pair phase). In fact, there are even points satisfying both $f_3 \geq 1-p_{n+3}$ and $f_0 \geq 1-p_n$, all of which belong to the $(n+2, n+1)$ -pair phase.

The $p_{n+3} + p_{n+2} + p_{n+1} = 1$ face of the pyramidal phase space of $\hat{\rho}_{4F}$ corresponds to the rank-3 case with populated photon numbers $n+3$, $n+2$, and $n+1$; the $(n+3)$ -triplet phase is a smooth extension of the lower-pair phase on this rank-3 face.

(n+1)-triplet—The $(n+1)$ -triplet phase is shown in the lower-left panel of Fig. 4. The optimal decomposition consists of one Fock state, $|n+1\rangle$, as well as states of the form:

$$|\phi_{1T}(\theta_j, \gamma_j, \zeta_j)\rangle = \sqrt{1-f_1}e^{i\gamma_j}|n+1\rangle + \sqrt{f_1}\left(\sqrt{\frac{p_{n+3}}{1-p_{n+1}}}|n+3\rangle + \sqrt{\frac{p_{n+2}}{1-p_{n+1}}}e^{i\theta_j}|n+2\rangle + \sqrt{\frac{p_n}{1-p_{n+1}}}e^{i\zeta_j}|n\rangle\right). \quad (42)$$

Such states contribute a total probability $(1-p_{n+1})f_1^{-1}$, which cannot exceed 1, and so $1 \geq f_1 \geq 1-p_{n+1}$. f_1 maximizes the objective, by making $(1-p_{n+1})f_1^{-1}|\langle\phi_{1T}(0,0,0)|\hat{a}|\phi_{1T}(0,0,0)\rangle|^2$ as large as possible. The ORT measure for states in this phase is:

$$\mathcal{N}(\hat{\rho}_{4F}) = 3p_{n+3} + 2p_{n+2} + p_{n+1} + n - (1-p_{n+1})f_1^{-1}|\langle\phi_{1T}(0,0,0)|\hat{a}|\phi_{1T}(0,0,0)\rangle|^2. \quad (43)$$

$f_1 = 1-p_{n+1}$ determines a boundary on this phase: note that $|\phi_{1T}(\theta_j, \gamma_j, \zeta_j)\rangle \rightarrow |\phi_Q(\theta_j, \gamma_j, \zeta_j)\rangle$ as $1-p_{n+1} \rightarrow f_1$. As far as we could determine from our numerical investigations, the $(n+1)$ -triplet decomposition is optimal for all points $(p_{n+3}, p_{n+2}, p_{n+1})$ in $1 \geq f_1 \geq 1-p_{n+1}$.

The $p_{n+3} + p_{n+2} + p_{n+1} = 1$ face of the pyramidal phase space of $\hat{\rho}_{4F}$ corresponds to the rank-3 case with populated photon numbers $n+3$, $n+2$, and $n+1$; the $(n+1)$ -triplet phase is a smooth extension of the upper-pair phase on this rank-3 face.

(n+2)-triplet—The $(n+2)$ -triplet phase is shown in the lower-middle panel of Fig. 4. The optimal decomposition consists of one Fock state, $|n+2\rangle$, as well as states

of the form:

$$\begin{aligned} |\phi_{2T}(\theta_j, \gamma_j, \zeta_j)\rangle &= \sqrt{1-f_2} e^{i\theta_j} |n+2\rangle \\ &+ \sqrt{f_2} \left(\sqrt{\frac{p_{n+3}}{1-p_{n+2}}} |n+3\rangle + \sqrt{\frac{p_{n+1}}{1-p_{n+2}}} e^{i\gamma_j} |n+1\rangle \right. \\ &\left. + \sqrt{\frac{p_n}{1-p_{n+2}}} e^{i\zeta_j} |n\rangle \right). \end{aligned} \quad (44)$$

Such states contribute a total probability $(1-p_{n+2})f_2^{-1}$, which cannot exceed 1, and so $1 \geq f_2 \geq 1-p_{n+2}$. f_2 maximizes the objective, by making $(1-p_{n+2})f_2^{-1} |\langle \phi_{2T}(0,0,0) | \hat{a} | \phi_{2T}(0,0,0) \rangle|^2$ as large as possible. The ORT measure for states in this phase is:

$$\begin{aligned} \mathcal{N}(\hat{\rho}_{4F}) &= 3p_{n+3} + 2p_{n+2} + p_{n+1} + n \\ &- (1-p_{n+2})f_2^{-1} |\langle \phi_{2T}(0,0,0) | \hat{a} | \phi_{2T}(0,0,0) \rangle|^2. \end{aligned} \quad (45)$$

$f_2 = 1-p_{n+2}$ determines a boundary on this phase: note that $|\phi_{2T}(\theta_j, \gamma_j, \zeta_j)\rangle \rightarrow |\phi_Q(\theta_j, \gamma_j, \zeta_j)\rangle$ as $1-p_{n+2} \rightarrow f_2$. As far as we could determine from our numerical investigations, the $(n+2)$ -triplet decomposition is optimal for all points $(p_{n+3}, p_{n+2}, p_{n+1})$ in $1 \geq f_2 \geq 1-p_{n+2}$.

The $p_{n+3} = 0$ face of the pyramidal phase space of $\hat{\rho}_{4F}$ corresponds to the rank-3 case with populated photon numbers $n+2$, $n+1$, and n ; the $(n+2)$ -triplet phase is a smooth extension of the lower-pair phase on this rank-3 face.

3. Pair Phase

The $(n+2, n+1)$ -pair phase is shown in the lower right panel of Fig. 4, and to our knowledge, is the only phase of its kind. This phase is in surface contact with the n -triplet and $(n+3)$ -triplet phases. The optimal decomposition breaks $\hat{\rho}_{4F}$ into two parts: one part has support only for $|n+3\rangle$ and $|n\rangle$ (any decomposition is optimal for this part), while the other part is optimally decomposed into states of the form:

$$\begin{aligned} |\phi_P(\theta_j, \gamma_j, \zeta_j)\rangle &= \sqrt{1-f} \left(\sqrt{g} |n+3\rangle + \sqrt{1-g} e^{i\zeta_j} |n\rangle \right) + \\ &\sqrt{f} \left(\sqrt{\frac{p_{n+2}}{p_{n+2}+p_{n+1}}} e^{i\theta_j} |n+2\rangle + \sqrt{\frac{p_{n+1}}{p_{n+2}+p_{n+1}}} e^{i\gamma_j} |n+1\rangle \right), \end{aligned} \quad (46)$$

where:

$$g = \frac{(3+n)p_{n+2}}{(1+n)p_{n+1} + (3+n)p_{n+2}} \quad (47)$$

and $f = f(n, p_{n+2}, p_{n+1})$ maximizes $(p_{n+2} + p_{n+1})f^{-1} |\langle \phi_P(0,0,0) | \hat{a} | \phi_P(0,0,0) \rangle|^2$. These states contribute a total probability $(p_{n+2} + p_{n+1})f^{-1}$. Interestingly, f and g depend only on n , p_{n+2} , and p_{n+1} (not on p_{n+3} or p_n). Consequently,

$(p_{n+2} + p_{n+1})f^{-1} |\langle \phi_P(0,0,0) | \hat{a} | \phi_P(0,0,0) \rangle|^2$ depends only on n , p_{n+2} , and p_{n+1} . The ORT measure in this phase is:

$$\begin{aligned} \mathcal{N}(\hat{\rho}_{4F}) &= 3p_{n+3} + 2p_{n+2} + p_{n+1} + n \\ &- (p_{n+2} + p_{n+1})f^{-1} |\langle \phi_P(0,0,0) | \hat{a} | \phi_P(0,0,0) \rangle|^2. \end{aligned} \quad (48)$$

This regime is bounded by the inequalities:

$$p_{n+2} + p_{n+1} \leq f \quad (49)$$

$$(1-f)f^{-1}g(p_{n+2} + p_{n+1}) \leq p_{n+3} \quad (50)$$

$$(1-f)f^{-1}(1-g)(p_{n+2} + p_{n+1}) \leq p_n. \quad (51)$$

Respectively, these inequalities ensure the $|\phi_P(\theta_j, \gamma_j, \zeta_j)\rangle$ states do not over-fill the total population, $|n+3\rangle$ population, and $|n\rangle$ population.

Lastly, we note that the $(n+2, n+1)$ -pair phase may be regarded as a further refinement of the n -triplet and $(n+3)$ -triplet phases. It lies within the union of $f_1 \geq 1-p_{n+1}$ and $f_3 \geq 1-p_{n+3}$ and covers the intersection of $f_1 \geq 1-p_{n+1}$ and $f_3 \geq 1-p_{n+3}$. Within its domain of validity, the $(n+2, n+1)$ -pair decomposition is superior to that of the corresponding triplet phases.

As far as we were able to determine from our numerical investigations, these six phases are the only six in the rank-4 case. We do not have an analytical proof, and of course could only check a finite number of parameter choices $(p_{n+3}, p_{n+2}, p_{n+1})$, so these ansatz may be considered conjectures. In support of our results, however, we note that there is a high degree of consistency to them, particularly in regards to how they map down to the rank-3 case.

C. Higher-rank cases

To demonstrate the scope of our linear programming numerical method, we apply it to higher-rank mixed Fock states of the form given by Eq. (17). As an example, we consider truncated thermal states, where the populations of $|n\rangle$ ($n \geq M$) are reduced to zero:

$$\hat{\rho}_{MF} = \sum_{k=0}^{M-1} p_k |k\rangle \langle k|, \quad (52)$$

where the populations are:

$$p_k = \mathcal{A} \frac{n_{\text{th}}^k}{(1+n_{\text{th}})^{k+1}} \quad (53)$$

with n_{th} the mean photon number of the field before the truncation and:

$$\mathcal{A} = \frac{1}{1 - \left(\frac{n_{\text{th}}}{1+n_{\text{th}}} \right)^M} \quad (54)$$

is the normalization factor after truncating the thermal states. Even though true (i.e., untruncated) thermal states are diagonal in the Fock basis, they are classical, meaning $\mathcal{N} = 0$ and their P -function is positive. This classicality is only possible because their expansion in terms of Fock states has infinitely many terms, which can be equivalently represented by a mixture of coherent states [30]. For truncated thermal states, they should evaluate nonclassicality.

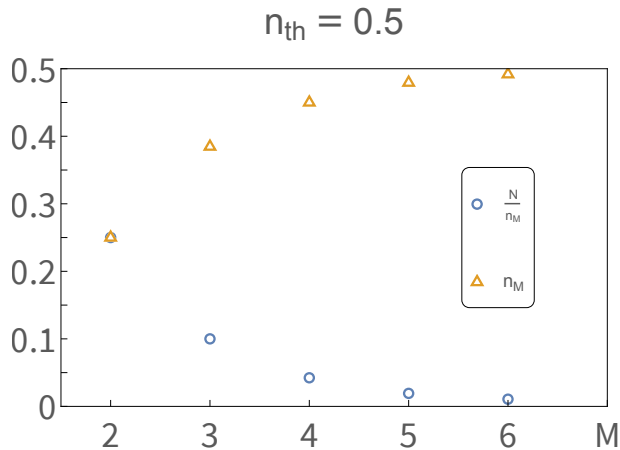


FIG. 5. Nonclassicality per unit average energy, \mathcal{N}/n_M , along with average energy n_M , of truncated thermal states. The original thermal state has average energy $n_{th} = 0.5$ and the truncated thermal states are obtained by projecting out all photon numbers greater than or equal to M . Such truncated thermal states should resemble the original thermal state (which has nonclassicality 0) more and more as M increases, and indeed we see $\mathcal{N}/n_M \rightarrow 0$ as M increases.

Increasing the number of terms in a truncated thermal state should cause the nonclassicality to approach zero (i.e., recovers the thermal state’s classicality). We demonstrate this in Fig. 5, where we evaluate the ORT measure, per unit average energy, using our numerical method in the rank-5 and rank-6 cases. We choose a low $n_{th} = 0.5$ such that the expected photon number after truncation at $M = 6$ is close to n_{th} : $n_6 = 0.491758$. Nonclassicality per unit energy \mathcal{N}/n_M indeed decreases from its $M = 2$ value of 0.25 to a $M = 6$ value of $\lesssim .011$.

D. Optimal Decompositions and Convexity

Before concluding, we would like to remark on a mathematical observation about our results. The insights here not only support our claims (about the optimal decompositions we found), but may be helpful for solving or checking the solution of other convex roof optimization problems.

The optimal decompositions we discovered may be divided into two categories: “simple” and “composite.” Examples of “simple” decompositions are the triplet decom-

position in the rank-3 case and the quartet decomposition in the rank-4 case. Recall that these decompositions are always *valid* regardless of the specific populations, although they may not be optimal (in the ORT measure sense). A state is “simply-decomposed” if its optimal decomposition is a simple decomposition: for example, $0.4|2\rangle\langle 2| + 0.4|1\rangle\langle 1| + 0.2|0\rangle\langle 0|$ is simply-decomposed since it lies in the triplet phase (see Fig. 2). Equivalently, a state is simply-decomposed if Eq. (23) is saturated. By contrast, $\hat{\rho}_{comp} = 0.2|2\rangle\langle 2| + 0.2|1\rangle\langle 1| + 0.6|0\rangle\langle 0|$ is not simply-decomposed, since it lies in the upper-pair phase (Fig. 2). Nevertheless, $\hat{\rho}_{comp}$ may be rewritten as a convex combination of density matrices that *are* simply-decomposed (it is “compositely-decomposed”): $\hat{\rho}_{comp.} = p_1\hat{\rho}_{simp,1} + p_2\hat{\rho}_{simp,2}$. In this case $\hat{\rho}_{simp,1} = |0\rangle\langle 0|$, $\hat{\rho}_{simp,2} = 0.25|2\rangle\langle 2| + 0.25|1\rangle\langle 1| + 0.5|0\rangle\langle 0|$, $p_1 = 0.2$, and $p_2 = 0.8$ — interestingly, $\hat{\rho}_{simp,2}$ is precisely at the boundary of the triplet and upper-pair phases (Fig. 2). The upper-pair decomposition of $\hat{\rho}_{comp.}$ makes precise use of this convex combination, see Eq. (26) and (27). Recall that the ORT measure satisfies convexity, meaning $\sum_j p_j \mathcal{N}(\hat{\rho}_j) \geq \mathcal{N}(\sum_j p_j \hat{\rho}_j)$ for any quantum states $\hat{\rho}_j$ and probabilities p_j . The equality can hold because the second term in Eq. (3) vanishes for the mixed Fock states. In this case, the equality holds if and only if the decomposition into $\hat{\rho}_j$ and probabilities p_j is optimal. A simple and important test for our proposed decompositions is that they saturate this inequality. In section III, we implied (however indirectly) that $\hat{\rho}_{comp.} = p_1\mathcal{N}(\hat{\rho}_{simp,1}) + p_2\mathcal{N}(\hat{\rho}_{simp,2})$, and so our analytical results pass this test.

These observations hold quite generally across all of our analytical results in the rank-3 and rank-4 cases. Rank-3 states in the triplet phase are simply-decomposed, and rank-4 states in the quartet phase are simply-decomposed. All other rank-3 and rank-4 states are compositely-decomposed, and may be thought of as convex combinations of simply-decomposed states (particularly states which lie at the boundaries of the simple phases). We fully expect these patterns to hold in higher-rank cases as well, although we did not derive any analytical results for them.

V. CONCLUSION

In this work, we introduced a method, based on linear programming, for evaluating the ORT measure of Fock-diagonal mixed states. In doing so, we have further advanced the ORT measure as a useful tool for characterizing bosonic nonclassicality. Our work also suggests that linear programming may be useful for solving convex roof optimization problems in other contexts, such as entanglement quantification.

We have provided in-depth results for the case where three or four neighboring Fock states are populated. Full solutions were obtained by carefully analyzing the opti-

mal histograms given by the linear programming method. We found that, depending on the populations, Fock-diagonal states can be in various different phases, wherein different types of decompositions are optimal (for ORT measure purposes). We also noted that the optimal decompositions we found fall into two categories: “simple” and “composite,” and that this distinction may be useful for solving other convex roof optimization problems.

We gave some numerical results for rank-5 and rank-6 states, showing that the method remains applicable. As the rank increases, the computational complexity does increase, as more bins are needed for the optimal histogram to be accurate. However, we suspect that such a challenge can be met by employing an iterative, adaptive approach.

Since the ORT measure is resource-theoretic, and re-

lated to metrological power, our results help facilitate deeper understanding of the resources behind quantum-enhanced sensing. Moving forward, we would like to use our results to study the tradeoff between entanglement generation and individual mode nonclassicality in a beam-splitter [12, 35–37]. We would also like to calculate the nonclassicality of mixed states that have coherences in the Fock basis.

ACKNOWLEDGEMENTS

We thank Luke Ellert-Beck and Garrett Jepson for helpful discussions.

This research is supported by NSF Award 2243591.

-
- [1] M. Hillery, Classical pure states are coherent states, *Physics Letters A* **111**, 409 (1985).
- [2] S. L. Braunstein and H. J. Kimble, Teleportation of continuous quantum variables, *Phys. Rev. Lett.* **80**, 869 (1998).
- [3] S. L. Braunstein and P. Van Loock, Quantum information with continuous variables, *Rev. Mod. Phys.* **77**, 513 (2005).
- [4] M. Mirrahimi, Z. Leghtas, V. V. Albert, S. Touzard, R. J. Schoelkopf, L. Jiang, and M. H. Devoret, Dynamically protected cat-qubits: a new paradigm for universal quantum computation, *New J. Phys.* **16**, 045014 (2014).
- [5] V. Giovannetti, S. Lloyd, and L. Maccone, Quantum metrology, *Phys. Rev. Lett.* **96**, 010401 (2006).
- [6] J. Aasi, J. Abadie, B. Abbott, R. Abbott, T. Abbott, M. Abernathy, C. Adams, T. Adams, P. Addesso, R. Adhikari, *et al.*, Enhanced sensitivity of the ligo gravitational wave detector by using squeezed states of light, *Nat. Photonics* **7**, 613 (2013).
- [7] M. Tse, H. Yu, N. Kijbunchoo, A. Fernandez-Galiana, P. Dupej, L. Barsotti, C. Blair, D. Brown, S. Dwyer, A. Effler, *et al.*, Quantum-enhanced advanced ligo detectors in the era of gravitational-wave astronomy, *Phys. Rev. Lett.* **123**, 231107 (2019).
- [8] C. T. Lee, Measure of the nonclassicality of nonclassical states, *Phys. Rev. A* **44**, R2775 (1991).
- [9] P. Marian, T. A. Marian, and H. Scutaru, Quantifying nonclassicality of one-mode gaussian states of the radiation field, *Physical Rev. Lett.* **88**, 153601 (2002).
- [10] M. Hillery, Nonclassical distance in quantum optics, *Phys. Rev. A* **35**, 725 (1987).
- [11] C. Gehrke, J. Sperling, and W. Vogel, Quantification of nonclassicality, *Phys. Rev. A* **86**, 052118 (2012).
- [12] W. Vogel and J. Sperling, Unified quantification of nonclassicality and entanglement, *Phys. Rev. A* **89**, 052302 (2014).
- [13] K. C. Tan, T. Volkoff, H. Kwon, and H. Jeong, Quantifying the coherence between coherent states, *Physical Rev. Lett.* **119**, 190405 (2017).
- [14] B. Yadin, F. C. Binder, J. Thompson, V. Narasimhachar, M. Gu, and M. S. Kim, Operational resource theory of continuous-variable nonclassicality, *Phys. Rev. X* **8**, 041038 (2018).
- [15] H. Kwon, K. C. Tan, T. Volkoff, and H. Jeong, Nonclassicality as a quantifiable resource for quantum metrology, *Phys. Rev. Lett.* **122**, 040503 (2019).
- [16] W. Ge, K. Jacobs, S. Asiri, M. Foss-Feig, and M. S. Zubairy, Operational resource theory of nonclassicality via quantum metrology, *Phys. Rev. Research* **2**, 023400 (2020).
- [17] W. Ge and M. S. Zubairy, Evaluating single-mode nonclassicality, *Phys. Rev. A* **102**, 043703 (2020).
- [18] W. Ge, K. Jacobs, and M. S. Zubairy, The power of microscopic nonclassical states to amplify the precision of macroscopic optical metrology, *npj Quantum Information* **9**, 5 (2023).
- [19] E. Chitambar and G. Gour, Quantum resource theories, *Rev. Mod. Phys.* **91**, 025001 (2019).
- [20] J. Merlin, E. Devibala, and A. B. M. Ahmed, Operational resource measure of nonclassicality for number states filtered coherent states, *Eur. Phys. J. D* **76**, 47 (2022).
- [21] M. D. Lang and C. M. Caves, Optimal quantum-enhanced interferometry using a laser power source, *Phys. Rev. Lett.* **111**, 173601 (2013).
- [22] G. Ferrini, D. Spehner, A. Minguzzi, and F. W. J. Hekking, Noise in bose josephson junctions: Decoherence and phase relaxation, *Phys. Rev. A* **82**, 033621 (2010).
- [23] A. Arqand, L. Memarzadeh, and S. Mancini, Quantum capacity of a bosonic dephasing channel, *Phys. Rev. A* **102**, 042413 (2020).
- [24] M. Strzalka, R. Filip, and K. Roszak, Qubit-environment entanglement in time-dependent pure dephasing, *Phys. Rev. A* **109**, 032412 (2024).
- [25] G. Tóth, T. Moroder, and O. Gühne, Evaluating convex roof entanglement measures, *Phys. Rev. Lett.* **114**, 160501 (2015).
- [26] K. Chen, S. Albeverio, and S.-M. Fei, Entanglement of formation of bipartite quantum states, *Phys. Rev. Lett.* **95**, 210501 (2005).
- [27] S. L. Braunstein and C. M. Caves, Statistical distance and the geometry of quantum states, *Phys. Rev. Lett.* **72**, 3439 (1994).
- [28] R. J. Glauber, The quantum theory of optical coherence, *Phys. Rev.* **130**, 2529 (1963).

- [29] E. C. G. Sudarshan, Equivalence of semiclassical and quantum mechanical descriptions of statistical light beams, *Phys. Rev. Lett.* **10**, 277 (1963).
- [30] M. O. Scully and M. S. Zubairy, *Quantum Optics* (Cambridge University Press, New York, 1997).
- [31] C. T. Lee, Measure of the nonclassicality of nonclassical states, *Phys. Rev. A* **44**, R2775 (1991).
- [32] G. Tóth and I. Apellaniz, Quantum metrology from a quantum information science perspective, *J. Phys. A: Math. Theor.* **47**, 424006 (2014).
- [33] K. Audenaert, F. Verstraete, and B. De Moor, Variational characterizations of separability and entanglement of formation, *Phys. Rev. A* **64**, 052304 (2001).
- [34] S. P. Boyd and L. Vandenberghe, *Convex Optimization* (Cambridge University Press, 2004).
- [35] W. Ge, M. E. Tasgin, and M. S. Zubairy, Conservation relation of nonclassicality and entanglement for gaussian states in a beam splitter, *Phys. Rev. A* **92**, 052328 (2015).
- [36] I. I. Arkhipov, J. Peřina Jr., J. Svozilík, and A. Miranowicz, Nonclassicality invariant of general two-mode gaussian states, *Scientific Reports* **6**, 26523 EP (2016).
- [37] J. Liu, W. Ge, and M. S. Zubairy, Classical-nonclassical polarity of gaussian states, arXiv preprint arXiv:2310.12104 (2023).